

# Heavy charged Higgs boson production at next generation $e^\pm\gamma$ colliders

---

**Shinya Kanemura**

*Physics and Astronomy Department, Michigan State University  
East Lansing, MI 48824-1116, USA*

**Stefano Moretti**

*Theory Division, CERN, CH-1211 Genève 23, Switzerland*

**Kosuke Odagiri**

*Theory Group, KEK, 1-1 Oho, Tsukuba, Ibaraki 305-0801, Japan*

**ABSTRACT:** We assess the potential of future electron-positron linear colliders operating in the  $e^\pm\gamma$  mode in detecting charged Higgs bosons with mass around and larger than the top quark mass, using Compton back-scattered photons from laser light. We compare the pair production mode,  $e^-\gamma \rightarrow e^-H^+H^-$ , to a variety of channels involving only one charged Higgs scalar in the final state, such as the tree-level processes  $e^-\gamma \rightarrow \nu_e H^- \Phi^0$  ( $\Phi^0 = h^0, H^0$  and  $A^0$ ) and  $e^-\gamma \rightarrow \nu_e f \bar{f} H^-$  ( $f = b, \tau$  and  $\nu_\tau$ ) as well as the loop-induced channel  $e^-\gamma \rightarrow \nu_e H^-$ . We show that, when the charged Higgs boson mass is smaller than or comparable to half the collider energy,  $\sqrt{s_{ee}} \gtrsim 2M_{H^\pm}$ , single production cross sections are of the same size as the pair production rate, whereas, for charged Higgs boson masses larger than  $\sqrt{s_{ee}}/2$ , all processes are heavily suppressed. In general, production cross sections of charged Higgs bosons via  $e^\pm\gamma$  scatterings are smaller than those induced at an  $e^+e^-$  collider and the latter represents a better option to produce and analyse such particles.

**KEYWORDS:** Supersymmetric Models, Higgs Physics, Linear colliders.

---

## Contents

1. Motivation	1
2. Production cross sections	3
3. Possible signals and detection strategies	6
4. Conclusions	8

---

## 1. Motivation

The physics case for exploiting the  $\gamma\gamma$  and  $e^\pm\gamma$  beam options of future electron-positron linear colliders (LCs) in testing the Higgs sector of the electroweak interactions is quite strong [1]. The scenario that one may well imagine as the legacy of the Large Hadron Collider (LHC) era could be the following. A neutral Higgs signal is detected at the CERN hadron collider, but no other particles are found, and all measurements of the parameters related to the new state (mass, width, couplings, etc.) are consistent with those of both, e.g., the Standard Model (SM) Higgs boson,  $\phi$ , and the lightest of the Minimal Supersymmetric Standard Model (MSSM) Higgs bosons,  $h^0$ . (This scenario corresponds in the MSSM to the so-called ‘decoupling regime’, when the additional Higgs states,  $H^0, A^0$  and  $H^\pm$ , are much heavier than the  $h^0$ .)

Since, to be optimistic, one should expect in the rather messy hadronic environment of the LHC no more than a 10% precision in the measurements of most of the Higgs boson couplings to ordinary matter (quarks, leptons and gauge vector bosons), it is reasonable to argue that one may have to wait till the advent of a future leptonic machine in order to be able to pin down the exact nature of the Higgs sector<sup>1</sup>. In fact, at future  $e^+e^-$  LCs, operating in the energy range  $\sqrt{s_{ee}} = 500$  to 1000 GeV, the accuracy of the same measurements is expected to improve to the level of 1% or even less [1, 3]. Besides, one can efficiently convert these machines to operate in the  $\gamma\gamma$  and  $e^\pm\gamma$  modes. By using Compton back-scattering of a few MeV laser light [4], one gets a spectrum of high energy photons which emerge with mean energy  $E_\gamma \approx 0.8E_{e^\pm}$ ,

---

<sup>1</sup>The precision of mass and width measurements in the two collider environments can become comparable in some instances, at least for the SM Higgs particle [2].

typical spread  $\langle \Delta E_\gamma \rangle \approx 0.07 E_\gamma$  and luminosity  $\mathcal{L}_{\gamma\gamma/e\gamma}(x > 0.8x_{\max}) \approx \frac{1}{3}\mathcal{L}_{ee}$ , where  $x \equiv \sqrt{s_{\gamma\gamma/e\gamma}}/\sqrt{s_{ee}}$  and  $x_{\max}$  will be given in eq. (2.3) (see Ref. [1] for details).

Under these circumstances, one could conceivably perform high precision measurements of the ‘Higgs –  $\gamma - \gamma$ ’ vertex<sup>2</sup> in either  $\gamma\gamma$  [5] or  $e^\pm\gamma$  collisions and of the ‘Higgs –  $\gamma - Z$ ’ one in the latter. Deviations in their experimental determinations from the values predicted by the SM can be considered as a signal of New Physics [6]<sup>3</sup>. From now on, we will assume that the underlying dynamics of the Higgs sector is the one of the MSSM and will start by summarising the Higgs discovery potential of the  $\gamma\gamma$  and  $e^\pm\gamma$  options of future LCs within this particular model.

The  $\gamma\gamma$  mode can profitably be exploited in the search for other Higgs boson states, in addition to the scalar  $h^0$ , via the same reaction which produces the latter<sup>4</sup>,  $\gamma\gamma \rightarrow \Phi^0$  [7]. Besides, the  $\gamma\gamma \rightarrow H^+H^-$  production mode [8] of charged Higgs scalars has a cross section larger than the one of the  $e^+e^-$  initiated mode [9]. As for the  $e^\pm\gamma$  case, other than via  $e^-\gamma \rightarrow e^-\Phi^0$  [10], one can access neutral Higgs states via the processes  $e^-\gamma \rightarrow e^-Z^0\Phi^0$ ,  $e^-\gamma \rightarrow \nu_e W^-\Phi^0$  and  $e^-\gamma \rightarrow \nu_e H^-\Phi^0$ , with the latter mode serving also the purpose of generating charged Higgs scalars, alongside the pair production channel  $e^-\gamma \rightarrow e^-H^+H^-$  [11] (see also [12]). Furthermore, the loop-induced production process  $e^-\gamma \rightarrow \nu_e H^-$  is an interesting possibility [13], which has been shown to yield sizable rates for small values of  $\tan\beta$ , though difficult to detect because of the SM continuum background. For both photonic environments, a detailed phenomenological simulation (at hadron and detector level), similar to those already carried out for the  $e^+e^-$  mode, see Refs. [3, 14], does not exist to date.

It is the purpose of our study to further elaborate on the potential of future LCs operating in the  $e^\pm\gamma$  mode in detecting  $H^\pm$  states, by looking at the case in which the mass of the charged Higgs boson of the MSSM is not only heavy (i.e., near or above the top mass,  $m_t$ ), as dictated by the mentioned decoupling scenario, but also near or above half the centre-of-mass (CM) energy of the collider, where the pair production modes of neutral and charged Higgs bosons have exhausted their potential, because of phase space suppression. In fact, for light enough  $M_{H^\pm}$  values (i.e., below  $m_t$ ), the processes

$$e^-\gamma \rightarrow e^-H^+H^- \quad (1.1)$$

and

$$e^-\gamma \rightarrow \nu_e H^-\Phi^0 \quad (1.2)$$

have already been proved to offer some chances in detecting such elusive particles [11]. When  $M_{H^\pm} \gtrsim m_t$ , they can both still be exploited, but the latter only when

---

<sup>2</sup>Here, ‘Higgs’ signifies either  $\phi$  or  $h^0$ .

<sup>3</sup>Recall that these vertices occur at one-loop level in both models and can be mediated by new virtual MSSM charged (s)particles.

<sup>4</sup>Hereafter, the symbol  $\Phi^0$  collectively refers to the three neutral Higgs boson states of the MSSM.

$\Phi^0 \equiv H^0$  or  $A^0$ , the  $h^0$  case being suppressed as in the heavy  $M_{H^\pm}$  case the  $h^0$  quickly decouples from the rest of the Higgs sector, see Fig. 7 of Ref. [11]. Here, in addition to the two modes (1.1)–(1.2), we also consider the channels

$$e^- \gamma \rightarrow \nu_e f \bar{f} H^-, \quad (1.3)$$

where  $f = b, \tau$  or  $\nu_\tau$ , and

$$e^- \gamma \rightarrow \nu_e H^-. \quad (1.4)$$

In particular, we intend to investigate whether the last two production modes can adequately complement the first two, possibly providing an extended coverage in the charged Higgs sector of the MSSM, beyond the kinematic threshold  $\sqrt{s_{ee}} \approx 2M_{H^\pm} \approx M_{H^\pm} + M_{\Phi^0}$  (here,  $\Phi^0 = H^0, A^0$ , in the decoupling regime).

We are also interested in assessing whether fundamental couplings of the underlying Higgs model can be better measured through  $e^\pm \gamma$  reactions than in  $e^+ e^-$  processes, such as: the  $(\gamma)W^\pm H^\mp \Phi^0$  vertices, via (1.2), the Yukawa couplings to top and bottom quarks of both neutral and charged Higgs states, in (1.3), the ‘form factors’ of the vertex  $\gamma W^\pm H^\mp$ , via (1.4).

Our present effort is meant to complement the one carried out in Refs. [15] (see also [16]) and [17] for the case of  $e^+ e^-$  and  $\gamma\gamma$  collisions, respectively, hence providing a complete overview of the feasibility of detecting heavy charged Higgs states in a future LC environment.

Notice that processes (1.1)–(1.3) all occur at tree level, whereas (1.4) takes place at one loop as the  $\gamma W^\pm H^\mp$  vertex is forbidden at tree level because of gauge invariance. The Feynman graphs corresponding to the above reactions are shown in Figs. 1–4, respectively. Also notice that, in order to avoid double counting process (1.2), we have not included in the simulation of (1.3) final states the contribution of graphs proceeding via intermediate  $\nu_e H^- \Phi^0$  stages (i.e., the diagrams in Fig. 1.2, followed by  $\Phi^0 \rightarrow b\bar{b}$ ).

## 2. Production cross sections

We have computed the production cross sections for  $e^- \gamma \rightarrow e^- H^+ H^-$  and  $e^- \gamma \rightarrow \nu_e H^- \Phi^0$  by using the program originally developed in Ref. [11]; the  $e^- \gamma \rightarrow \nu_e f \bar{f} H^-$  reactions were simulated by producing a totally new code, based on helicity amplitudes [18]; finally, for  $e^- \gamma \rightarrow \nu_e H^-$  production, our code was based on that developed in Refs. [13, 19].

All processes were calculated at leading order only. For the SM parameters we adopted the following setup:  $m_b = 4.25$  GeV,  $m_t = 175$  GeV,  $m_e = 0.511$  MeV,  $m_\tau = 1.78$  GeV,  $m_\nu = 0$ ,  $M_W = 80.23$  GeV,  $\Gamma_W = 2.08$  GeV,  $M_Z = 91.19$  GeV,  $\Gamma_Z = 2.50$  GeV,  $\sin^2 \theta_W = 0.232$ . The top quark width  $\Gamma_t$  was evaluated at leading order for each value of  $M_{H^\pm}$  and  $\tan \beta$ . Neutral and charged Higgs masses were

calculated for given values of  $M_{A^0}$  and  $\tan\beta$  using the HDECAY package [20], with the SUSY masses, the trilinear couplings and the Higgsino mass parameter  $\mu$  being set to 1 TeV. The Higgs boson widths  $\Gamma_{H^\pm, \Phi^0}$  were all evaluated again by using the above package. In the one-loop analysis of process (1.4) we assumed that the superpartners are sufficiently heavy to decouple, so that only the heavy-quark loops and Higgs–gauge loops need to be included.

We have used the energy spectrum of the back-scattered (unpolarised) photon given by Ref. [4]

$$F_{\gamma/e}(x) = \frac{1}{D(\xi)} \left[ 1 - x + \frac{1}{1-x} - \frac{4x}{\xi(1-x)} + \frac{4x^2}{\xi^2(1-x)^2} \right], \quad (2.1)$$

where  $D(\xi)$  is the normalisation factor

$$D(\xi) = \left( 1 - \frac{4}{\xi} - \frac{8}{\xi^2} \right) \ln(1+\xi) + \frac{1}{2} + \frac{8}{\xi} - \frac{1}{2(1+\xi)^2}, \quad (2.2)$$

and  $\xi = 4E_0\omega_0/m_e^2$ , where  $\omega_0$  is the incoming laser photon energy and  $E_0$  the (unpolarised) positron one. In eq. (7)  $x = \omega/E_0$  is the fraction of the energy of the incident positron carried by the back-scattered photon, with a maximum value

$$x_{\max} = \frac{\xi}{1+\xi}. \quad (2.3)$$

In order to maximise  $\omega$  avoiding  $e^+e^-$  pair creation, one takes  $\omega_0$  such that  $\xi = 2(1+\sqrt{2})$ . So, we obtain the typical values  $\xi \simeq 4.8$ ,  $x_{\max} \simeq 0.83$ ,  $D(\xi) \simeq 1.8$ , with  $\omega_0 \simeq 1.25(0.63)$  eV for a  $\sqrt{s_{ee}} = 0.5(1)$  TeV  $e^+e^-$  collider. In the case of an  $e^\pm\gamma$  scattering the total cross section  $\sigma$  is obtained by folding the subprocess cross section  $\hat{\sigma}$  with the photon luminosity  $F_{\gamma/e}$ :

$$\sigma(s_{ee}) = \int_{x_{\min}}^{x_{\max}} dx F_{\gamma/e}(x) \hat{\sigma}(\hat{s}_{e\gamma} = xs_{ee}), \quad (2.4)$$

where  $\hat{s}_{e\gamma}$  is the center of mass (CM) energy at parton ( $e\gamma$ ) level, while

$$x_{\min} = \frac{(M_{\text{final}})^2}{s_{ee}}, \quad (2.5)$$

with  $M_{\text{final}}$  the sum of the final state particle masses.

We present the cross sections as functions of the charged Higgs boson mass  $M_{H^\pm}$  at collider energies of  $\sqrt{s_{ee}} = 500$  and 1000 GeV and four different values of  $\tan\beta$ , 1.5, 7, 30 and 40. This is done in Fig. 5 for the pair production process (1.1) — for which there exists no  $\tan\beta$  dependence, in fact — and in Figs. 6 to 8 for the single  $H^\pm$  modes. The  $\tan\beta$  dependence of processes (1.2)–(1.4) can be understood as follows. In  $e^-\gamma \rightarrow \nu_e H^- \Phi^0$  ( $\Phi^0 = h^0, H^0, A^0$ ), only couplings relevant to  $W^\pm$  bosons are involved. If we represent the Higgs fields in the gauge basis (through a

so-called ‘ $\beta$ -rotation’, i.e., a rotation of the mass matrix by the angle  $\beta$ , the ratio of the vacuum expectation values of the two MSSM Higgs doublets), we have two new doublets,  $H_{\text{SM}}$  (a SM-like one) and  $H_{\text{add}}$ ,

$$H_{\text{add}} = \begin{pmatrix} H^+ \\ (\phi_2^0 + iA^0)/\sqrt{2} \end{pmatrix}, \quad (2.6)$$

where the field  $\phi_2^0$  is a superposition of the physical mass eigenstates  $h^0$  and  $H^0$ , and is diagonalised through a rotation by the angle  $\alpha - \beta$ . From this formulation, it is clear that in the vertices  $W^\pm H^\mp \Phi^0$  only the cases  $\Phi^0 = h^0, H^0$  can carry a  $\tan\beta$  dependence. However, for large  $M_{H^\pm}$ , one has that  $\phi_2^0 \rightarrow H^0$ , so that such dependence disappears to a large extent also for the case  $\Phi^0 = H^0$ . (In other terms, as already mentioned, in the decoupling limit  $M_{H^\pm} \rightarrow \infty$ ,  $H^0$  carries the full gauge coupling dependence and  $h^0$  does decouple.) Furthermore, for  $e^- \gamma \rightarrow \nu_e f \bar{f} H^-$ , the  $\tan\beta$  dependence mainly comes from the  $H^\pm f \bar{f}'$  Yukawa couplings, with some minor contaminations due to  $\Phi^0 f \bar{f}$  vertices as well. There is also a resonant effect for  $f = b$ , in the region  $M_{H^\pm} \lesssim m_t$ , induced by  $\bar{t} \rightarrow \bar{b} H^-$  decays (see diagrams 2 and 6 in Fig. 3). Finally, in  $e^- \gamma \rightarrow \nu_e H^-$ , the  $H^\pm t \bar{b}$  Yukawa interaction is modulated by the chirality structure of the loop diagrams (top-bottom loop contributions are dominant in fact), so that in the end the  $\tan\beta$  dependence becomes  $\sim 1/\tan\beta$  or  $\sim m_b^2/m_t^2 \tan\beta$ , rather than  $\sim 1/\tan\beta^2$  or  $\sim m_b^2/m_t^2 \tan\beta^2$  (at amplitude level), for any  $M_{H^\pm}$ , this explaining the enhancement for low  $\tan\beta$  values.

If we assume, for instance, an integrated luminosity of  $500 \text{ fb}^{-1}$  (which could be collected after a few years running [1, 21]),  $10^{-5} \text{ pb}$  corresponds to 5 events before acceptance cuts and background reduction. We do not discuss the background reduction procedure in detail in this study, and  $10^{-5} \text{ pb}$  is taken naively as the threshold of the ‘relevance’ of a process to the study of charged Higgs production at an  $e^\pm \gamma$  LC. We emphasise that this is not intended in any way as a threshold of detectability, or even visibility, as the evaluation of such thresholds would require jet simulations and machine-dependent considerations which are clearly beyond the scope of the current study.

The most prolific production channel is surely  $e^- \gamma \rightarrow e^- H^+ H^-$ , for any value of  $M_{H^\pm}$  up to  $\sqrt{s_{ee}} \approx 2M_{H^\pm}$ . However, the contribution from all other single  $H^\pm$  production modes becomes comparable to that of the pair production mode. In fact, after 500 inverse femtobarns of luminosity have been collected, one may expect between 2,000 and 110  $H^+ H^-$  events to be produced, for  $M_{H^\pm}$  ranging between 140 GeV and  $0.4\sqrt{s_{ee}}$  when  $\sqrt{s_{ee}} = 500 \text{ GeV}$ , whereas corresponding numbers at 1000 GeV of CM energy are 6,000 and 20. The single  $H^\pm$  production channels can altogether furnish between 395 (122) [336] {490} and 14 (7) [12] {17} events at  $\sqrt{s_{ee}} = 500 \text{ GeV}$ , corresponding to  $M_{H^\pm} = 140$  and 200 GeV, respectively, for  $\tan\beta = 1.5$  (7) [30] {40}. At  $\sqrt{s_{ee}} = 1000 \text{ GeV}$ , one instead has 877 (683) [1357] {2201} events for  $M_{H^\pm} = 140 \text{ GeV}$  and 15 (2) [8] {13} for  $M_{H^\pm} = 400 \text{ GeV}$ .

Above the kinematic threshold of pair production, i.e., when  $2M_{H^\pm} \gtrsim 0.8\sqrt{s_{ee}}$ , only the loop-mediated process  $e^-\gamma \rightarrow \nu_e H^-$  can in principle be useful, at least at low  $\tan\beta$ . In fact, for  $\tan\beta = 1.5$ , one has 10 events when  $\sqrt{s_{ee}} = 500$  GeV and  $M_{H^\pm} = 300$  GeV, or  $\sqrt{s_{ee}} = 1000$  GeV and  $M_{H^\pm} = 600$  GeV. For such heavy masses, all other single  $H^\pm$  channels become negligible, even at large  $\tan\beta$ . Further notice the much steeper descent in the production rates of processes (1.2)–(1.3), Figs. 6–7, with respect to those of process (1.4), see Figs. 8, with growing Higgs mass values.

### 3. Possible signals and detection strategies

Over most of the heavy mass range,  $M_{H^\pm} \geq m_t$ , charged Higgs bosons decay to  $t\bar{b}$  (and charge conjugate) pairs [22]. Given the not so large production rates in all modes considered, it is natural to focus on this decay channel first<sup>5</sup>.

If both charged Higgs bosons decay to top-bottom pairs, the final signature produced by the  $H^+H^-$  production channel is  $b\bar{b}b\bar{b}W^+W^-$ <sup>6</sup>, with the very forward/backward electron escaping detection. Under these circumstances, one may apply the same selection procedure outlined in Ref. [14], for the  $e^+e^- \rightarrow H^+H^-$  case. Here, the two  $W^\pm$ 's are required to decay hadronically, hence, the final signal is made up by eight jets. Four of these can be  $b$ -tagged with high efficiency. Both  $W^\pm$ 's and  $t$ 's are reconstructed. After completing the jet assignment, one can finally perform a kinematical fit, imposing the constraint of equal Higgs boson masses. This way, the signal should clearly emerge from the background with high statistical significance. The latter is expected to mainly be constituted by  $e^-\gamma \rightarrow e^-t\bar{t}h^0$  events, with  $h^0 \rightarrow b\bar{b}$ , the counterpart of  $e^+e^- \rightarrow t\bar{t}h^0 \rightarrow t\bar{t}b\bar{b}$ , discussed in the above paper. Another noise could be induced in the  $e^\pm\gamma$  case by triple-gauge-vector production, via  $e^-\gamma \rightarrow e^-Z^0W^+W^-$ , with  $W^+W^- \rightarrow jjjj$  and  $Z \rightarrow jjjj$  too. This background can however be suppressed by imposing  $M_{jjjj} \neq M_{Z^0}$ , even before enforcing  $b$ -tagging. (Events of the type  $e^-\gamma \rightarrow \nu_e W^-W^+W^-$ , with a longitudinal  $W^-$  boson exchange, could in principle be relevant; in practise to impose  $b$ -tagging should be enough to remove them efficiently.)

The signature expected from the single  $H^\pm$  production modes (1.2)–(1.3) is either the one above, or else  $b\bar{b}b\bar{b}W^-$ , with  $W^- \rightarrow jj$ , yielding one less jet pair (again, assuming  $H^- \rightarrow t\bar{b}$  hadronic decays). On the one hand, it should be noticed that processes of the type (1.3) with  $f = \tau, \nu_\tau$  are smaller in comparison to the case  $f = b$ . On the other hand, for  $M_{\Phi^0}$  below 400 GeV, the dominant decays of neutral Higgs bosons

---

<sup>5</sup>In the pair production mode, one may alternatively conceive to ask for one of the two charged Higgs bosons to decay via  $H^- \rightarrow \tau\nu_\tau$ , assuming large  $\tan\beta$  values, where the corresponding Branching Ratio (BR) can be as large as 10% [22]. However, we do not consider here this possibility.

<sup>6</sup>The  $H^+H^- \rightarrow t\bar{t}b\bar{b}$  decay combination can be complemented by the  $H^+H^- \rightarrow W^+h^0W^-h^0$  one, at low  $\tan\beta$ , and mixtures of the four  $H^\pm$  decays modes, all producing the  $b\bar{b}b\bar{b}W^+W^-$  intermediate stage.

are either  $\Phi^0 \rightarrow b\bar{b}$  (yielding the six-jet signature) or  $H^0 \rightarrow h^0 h^0, W^+ W^-, Z^0 Z^0$  and  $A^0 \rightarrow Z^0 h^0$ , with  $h^0 \rightarrow b\bar{b}$  and  $W^\pm, Z^0 \rightarrow jj$  (yielding the eight-jet signature). Thus, one could pursue in either case a selection strategy along the lines already described, with the only caution of constraining the final kinematical fit to different intermediate masses ( $M_{h^0}$ ,  $M_{W^\pm}$  and/or  $M_{Z^0}$ , rather than a second  $m_t$ ). Unfortunately, in the single  $H^\pm$  production cases, one can no longer impose the equal Higgs mass constraints, which revealed itself rather effective in rejecting both combinatorial and genuine background in the  $e^+ e^- \rightarrow H^+ H^-$  case. Significant noises in the eight-jet channel are as above, whereas in the six-jet case one may expect  $e^- \gamma \rightarrow e^- t\bar{t}$  (again, the electron is assumed to be undetected), with  $t\bar{t} \rightarrow b\bar{b} W^+ W^-$  and  $W^+ W^-$  yielding in turn four jets, to be relevant. This can however be suppressed by a triple (at least)  $b$ -tagging and/or a mass rejection,  $M_{jj} \neq M_{W^\pm}$ , against a second jet-pair reconstructing a  $W^\pm$  mass.

The total production rate for the  $\nu_e b\bar{b} H^-$  final state can be found in Figs. 9 (upper curves). These have been computed by adding to the diagrams in Fig. 3 (for the case  $f = b$  and  $f' = t$ ) those in Fig. 2, the latter supplemented by the decay currents  $\Phi^0 \rightarrow b\bar{b}$  (including Higgs propagator effects), then taking the square of the sum of all such diagrams. This way, interference effects between the two channels are taken into account appropriately. In the total cross sections, one may appreciate the different components of  $b\bar{b} H^-$  final states. When  $M_{H^\pm} \lesssim m_t$ , there is a resonant contribution from  $\bar{t} \rightarrow \bar{b} H^-$  decays (graphs 2,5,7 and 11 in Fig. 3), which is clearly visible in the lower curves. The resonant  $\Phi^0 \rightarrow b\bar{b}$  contributions are responsible for the general increase of the production rates for  $M_{H^\pm} \lesssim \sqrt{s_{e\gamma}}/2$  (upper curves versus lower curves in Figs. 9). The relative strength of the two resonant contributions in the allowed kinematic regions is regulated by  $\tan \beta$  [22]. The contributions from the Higgs-strahlung diagrams, namely 3 and 8 in Fig. 3, is much smaller at both energies considered, and can yield rates in small excess of  $\mathcal{O}(10^{-5})$  fb only at  $\tan \beta = 40$  and  $M_{H^\pm} \lesssim m_t$ .

Process (1.4) has already been studied in Ref. [13], where a detailed signal-to-background analysis has been carried out, for the dominant charged Higgs decay channel, to top-bottom pairs, with respect the continuum production  $e^- \gamma \rightarrow \nu_e t\bar{b}$ . Unfortunately, despite the signal is above our threshold of relevance up to very large masses, well beyond  $\sqrt{s_{e\gamma}}/2$  (as already remarked), for both CM energy considered and at small  $\tan \beta$  (see Fig. 8), the mentioned irreducible noise is in the end prohibitive (besides, notice that the latter scales with  $\tan \beta$  exactly as the signal does, see Ref. [13]). Finally, it was also pointed out in the study of Ref. [13]) the negative interference effects between signal and background, which further deplete the signal-to-background rates.

To summarise our findings, the interesting production modes (1.1)–(1.4), which are specific to the  $e^\pm \gamma$  option, have cross sections which are too small to be of much use, and the quantities which can in principle be measured there (such as



multiple Higgs-gauge-boson and Higgs-fermion couplings) can be better accessed in  $e^+e^-$  collisions, as can be confirmed by comparing the results presented here with those obtained in Ref. [15].

## 4. Conclusions

We have verified that the potential of future LCs operating in the  $e^\pm\gamma$  mode in covering the heavy charged Higgs boson sector of the MSSM is only limited to values of the charged Higgs boson mass compatible with the kinematic constraint  $2M_{H^\pm} \lesssim \sqrt{s_{e\gamma}} \approx 0.8\sqrt{s_{ee}}$ . However, over this range, not only the pair production mode  $e^-\gamma \rightarrow e^-H^+H^-$  is large, but also a variety of single  $H^\pm$  production channels,  $e^-\gamma \rightarrow \nu_e H^-\Phi^0$  (when  $\Phi^0 = H^0$  and  $A^0$ ),  $e^-\gamma \rightarrow \nu_e b\bar{b}H^-$  and  $e^-\gamma \rightarrow \nu_e H^-$ , can produce rates of the same order of magnitude. In general, we have so far established that the  $e^+e^-$  beam option of future LCs offers better chances than the  $e^\pm\gamma$  one of detecting and studying heavy charged Higgs bosons of the MSSM (recall Ref. [15]). In fact, the arguments adopted here and in Ref. [15] can equally be applied to a more general Two-Higgs-Doublet-Model (2HDM).

The drawbacks of the  $e^\pm\gamma$  beam option in comparison to the  $e^+e^-$  are twofold. Firstly, Higgs cross sections are significantly smaller, both for pair production and single  $H^\pm$  channels. Secondly, when  $M_{H^\pm}$  is significantly larger than  $\sqrt{s_{e\gamma}}/2$  — so that  $H^+H^-$  final states are no longer available — none of the single production modes considered here is able to furnish enough events to pursue a statistically significant analysis. Not even the loop-induced mode  $e^-\gamma \rightarrow \nu_e H^-$  is very helpful. Here, despite the fact that the production rates are very stable up to very large  $M_{H^\pm}$  values (indeed, comparable to  $\sqrt{s_{e\gamma}}$ ) and that in principle the signal could be observable at very low  $\tan\beta$  (in which case though, one should dismiss the MSSM in favour of a general 2HDM), one has to cope with a large irreducible background in non-resonant  $e^-\gamma \rightarrow \nu_e t\bar{b}$  events, overwhelming the signal in the  $H^- \rightarrow t\bar{b}$  decay mode, even before taking into account the negative interference between the two competing processes [13]. This situation is in contrast with the case of single charged Higgs production at the  $e^+e^-$  option, where it has been revealed that there are several channels which are viable complements to the pair production mode [15].

Finally, although at the energy scales which we have considered in this work the  $e^\pm\gamma$  option offers no advantage compared to the  $e^+e^-$  one, the situation would get somewhat brighter at higher CM energies. We note that the cross sections typically behave as  $1/s_{ee}$  in annihilation reactions (i.e., in the  $e^+e^-$  option of a LC), whereas the  $t$ -channel induced  $e^\pm\gamma$  processes have cross sections which scale as  $\log(s_{e\gamma})$  with increasing energy. At 5 TeV [23], for example, we believe that the  $e^\pm\gamma$  option would offer physics opportunities that can complement those available in  $e^+e^-$  and  $\gamma\gamma$  LCs. However, we have not pursued here this possibility, as we have confined ourselves to current design values of  $\sqrt{s_{ee}}$  at TESLA [24], i.e., in the TeV region.

A similar analysis [17] to the one performed here and in Ref. [15] is now in progress for the  $\gamma\gamma$  beam option of future LCs.

## Acknowledgements

SK would like to thank C.-P. Yuan for useful discussions. SK and KO would like to thank KEK for enabling KO's visit to Osaka and for hospitality during SK's visit to KEK. SK and KO also thank Y. Okada for discussions.

## References

- [1] I.F. Ginzburg, preprint [hep-ph/9907549](#); E. Boos, A. De Roeck, I.F. Ginzburg, K. Hagiwara, R.D. Heuer, G. Jikia, J. Kwiecinski, D.J. Miller, T. Takahashi, V. Telnov, T. Rizzo, I. Watanabe and P.M. Zerwas, talk given at the *International Workshop on High Energy Photon Colliders*, June 14-17, 2000, DESY, Hamburg, Germany, preprint March 2001, [hep-ph/0103090](#).
- [2] V. Drollinger and A. Sopczak, to appear in *Proceedings of 5th International Linear Collider Workshop (LCWS 2000)*, Fermilab, Batavia, Illinois, 24-28 October 2000, preprint February 2001, [hep-ph/0102342](#).
- [3] M. Battaglia and K. Desch, to appear in *Proceedings of 5th International Linear Collider Workshop (LCWS 2000)*, Fermilab, Batavia, Illinois, 24-28 October 2000, preprint January 2001, [hep-ph/0101165](#).
- [4] V. Telnov, *Nucl. Instrum. Methods A* **294** (1990) 72; I. Ginzburg, G. Kotkin, V. Serbo and V. Telnov, *Nucl. Instrum. Methods A* **205** (1983) 47, *ibidem A* **219** (1984) 5.
- [5] M. Melles, to appear in *Proceedings of 5th International Linear Collider Workshop (LCWS 2000)*, Fermilab, Batavia, Illinois, 24-28 October 2000, preprint December 2000, [hep-ph/0012195](#).
- [6] A. Djouadi, V. Driesen, W. Hollik and A. Kraft *Eur. Phys. J. C* **1** (1998) 163; A. Djouadi, V. Driesen, W. Hollik and J.I. Illana, *Eur. Phys. J. C* **1** (1998) 149; E. Gabrielli, V.A. Ilyin and B. Mele, *Phys. Rev. D* **56** (1997) 5945, *Phys. Rev. D* **60** (1999) 113005; A.T. Banin, I.F. Ginzburg and I.P. Ivanov, *Phys. Rev. D* **59** (1999) 115001; G.J. Gounaris and F.M. Renard, *Z. Physik C* **69** (1996) 513.
- [7] J.F. Gunion, preprint UCD-93-8, March 1993, in *Erice 1992, 23rd Eloisatron workshop, Properties of SUSY particles*, page 279, [hep-ph/9303297](#).
- [8] D. Bowser-Chao, K. Cheung and S. Thomas, *Phys. Lett. B* **315** (1993) 399.
- [9] S. Komamiya, *Phys. Rev. D* **38** (1988) 2158.
- [10] O.J.P. Eboli and M.C. Gonzales-Garcia, *Phys. Rev. D* **49** (1994) 91.

- [11] S. Moretti, *Phys. Rev. D* **50** (1994) 2016.
- [12] E. Boos, M. Dubinin, V. Ilyin, A. Pukhov, G. Jikia and S. Sultanov, *Phys. Lett. B* **273** (1991) 173; K. Hagiwara, I. Watanabe and P. Zerwas, *Phys. Lett. B* **278** (1992) 187.
- [13] S. Kanemura and K. Odagiri, preprint KEK-TH-759, MSU-HEP-010401, hep-ph/0104179.
- [14] M. Battaglia, A. Kiiskinen and P. Poyhonen, to appear in *Proceedings of 5th International Linear Collider Workshop (LCWS 2000)*, Fermilab, Batavia, Illinois, 24-28 October 2000, preprint January 2001, hep-ph/0101239.
- [15] S. Kanemura, S. Moretti and K. Odagiri, *J. High Energy Phys.* **02** (2001) 011.
- [16] S. Kanemura, S. Moretti and K. Odagiri, to appear in *Proceedings of 5th International Linear Collider Workshop (LCWS 2000)*, Fermilab, Batavia, Illinois, 24-28 October 2000, preprint January 2001, hep-ph/0101354.
- [17] S. Kanemura, S. Moretti and K. Odagiri, in preparation.
- [18] H. Murayama, I. Watanabe and K. Hagiwara, KEK Report 91-11, January 1992.
- [19] S. Kanemura, *Eur. Phys. J. C* **17** (2000) 473.
- [20] A. Djouadi, J. Kalinowski and M. Spira, *Comput. Phys. Commun.* **108** (1998) 56.
- [21] For the TESLA design, see, e.g.:  
[http://www.desy.de/~njwalker/ecfa-desy-wg4/parameter\\_list.html](http://www.desy.de/~njwalker/ecfa-desy-wg4/parameter_list.html).
- [22] S. Moretti and W.J. Stirling, *Phys. Lett. B* **B347** (1995) 291, Erratum, *ibidem* **B 366** (1996) 451.
- [23] See, e.g.:  
M. Battaglia, preprint LC-PHSM-2001-072-CLIC, March 2001, hep-ph/0103338.
- [24] See, e.g.:  
<http://www.desy.de/~lcnotes/tdr>.

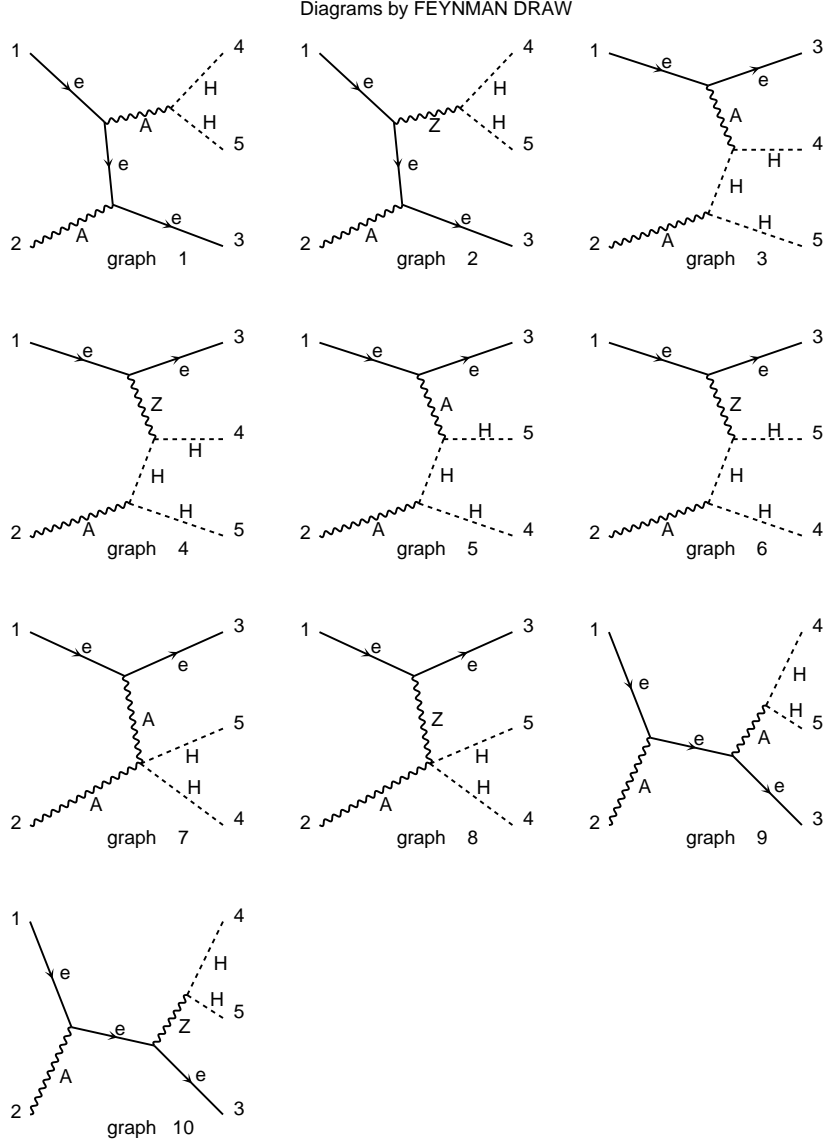


**Figure 1:** Feynman diagrams for process (1.1). The labels  $e$ ,  $A$ ,  $Z$  and  $H$  refer to an electron,  $\gamma$ ,  $Z$  and to both neutral and charged Higgs bosons, as appropriate, respectively.

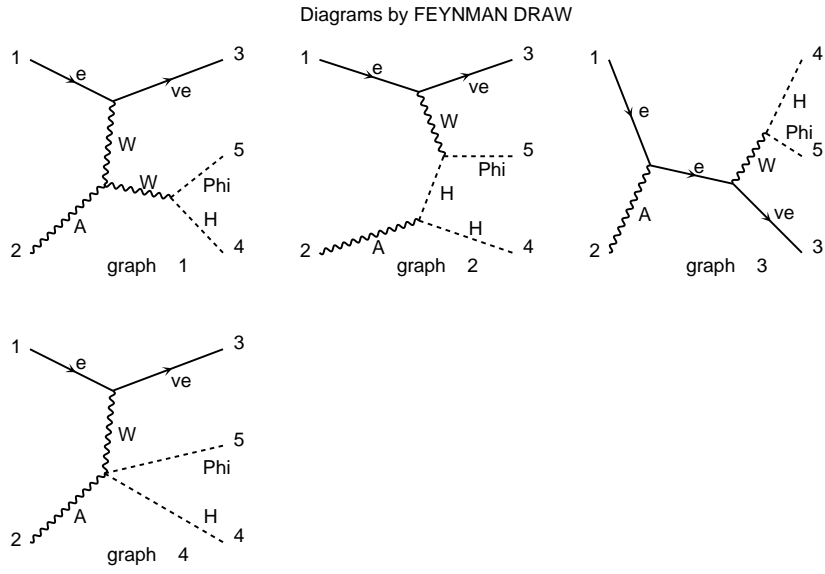


**Figure 2:** Feynman diagrams for processes of the type (1.2). The labels  $e$ ,  $\nu_e$ ,  $A$ ,  $W$  and  $H(\Phi)$  refer to an electron, neutrino,  $\gamma$ ,  $W^\pm$  and a charged(neutral) Higgs boson, respectively.

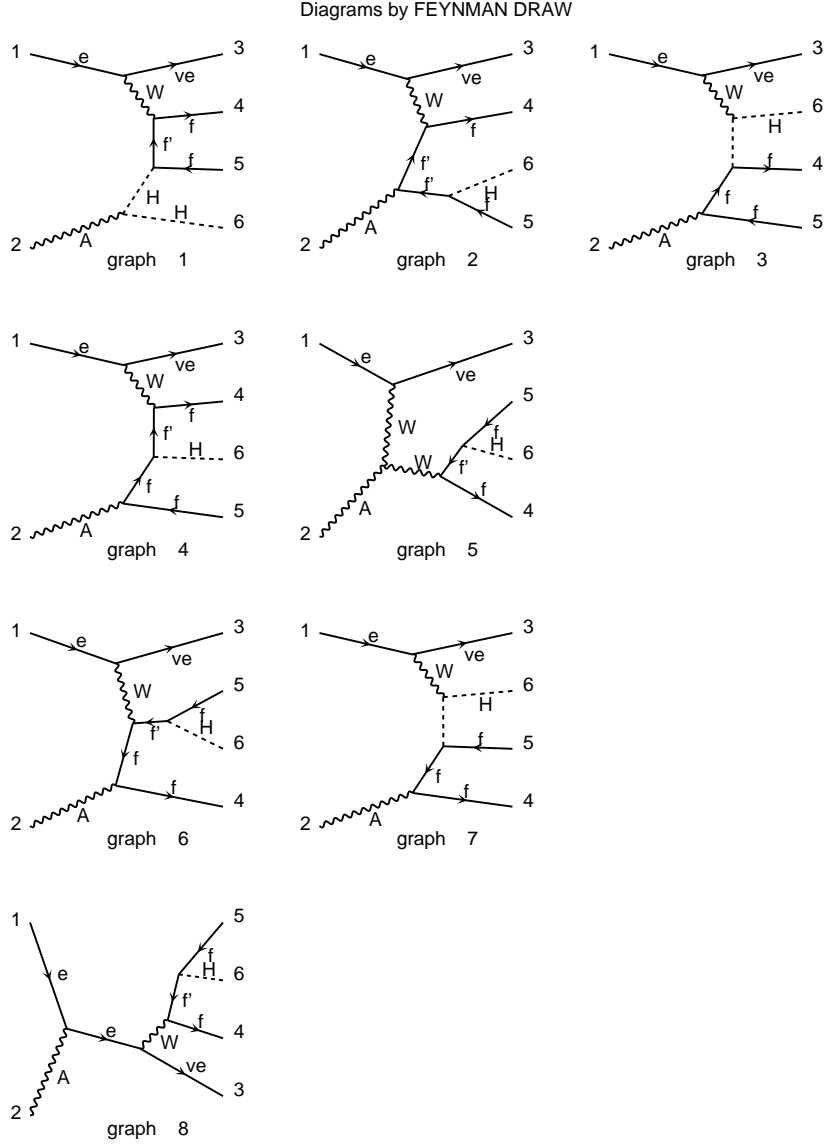


**Figure 3:** Feynman diagrams for processes of the type (1.3). The labels  $e$ ,  $\nu_e$ ,  $A$ ,  $W$  and  $H$  refer to an electron, neutrino,  $\gamma$ ,  $W^\pm$  and a charged Higgs boson, respectively, whereas  $f'$  and  $f$  refer to  $b$ - and  $t$ -quarks or  $\tau$ - and  $\nu_\tau$ -leptons, as appropriate.

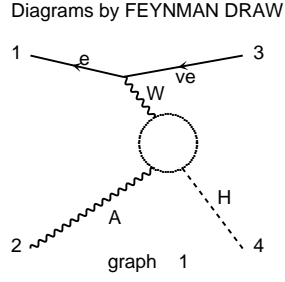


**Figure 4:** Feynman diagrams for processes of the type (1.4). Labels are as in Fig. 2 (apart from  $\Phi$ ). The loop particle content is detailed in Ref. [19].

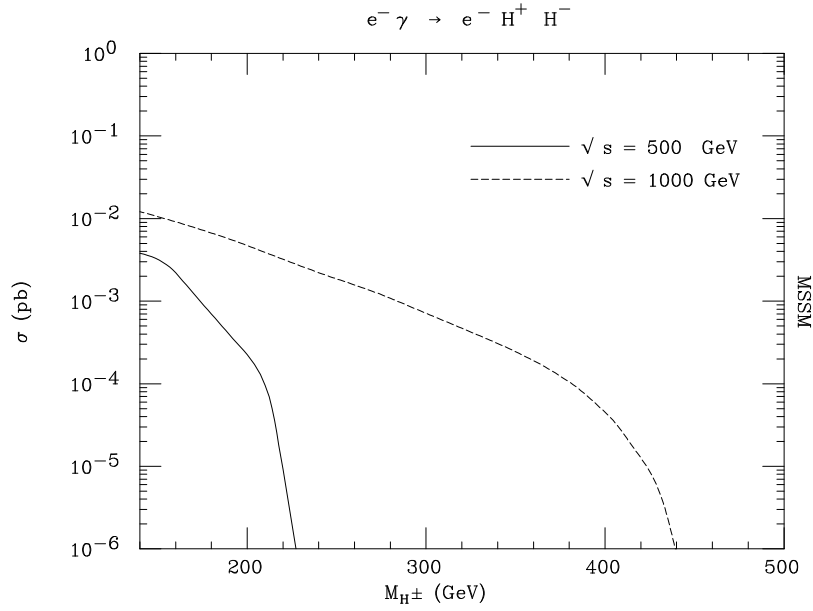
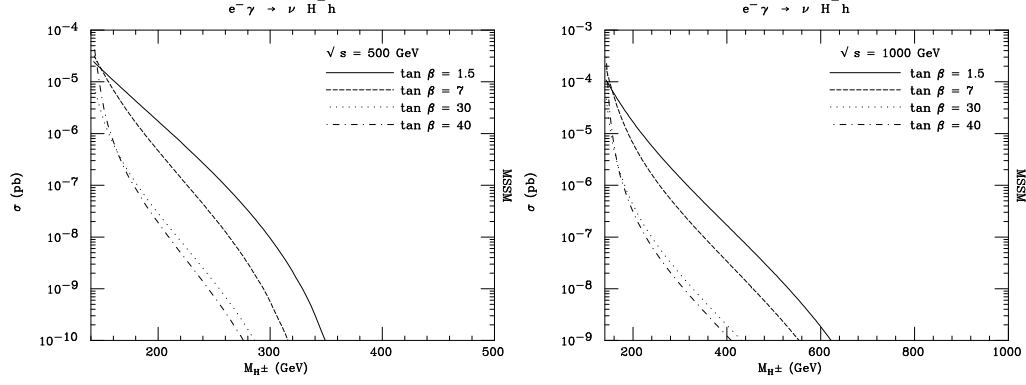
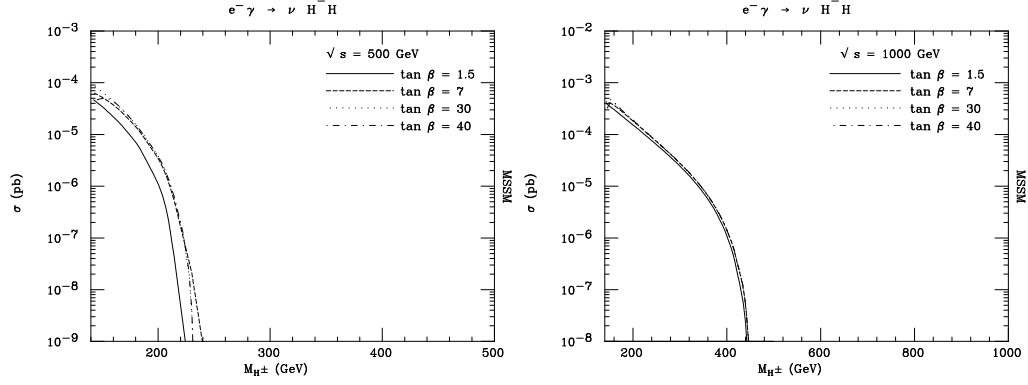


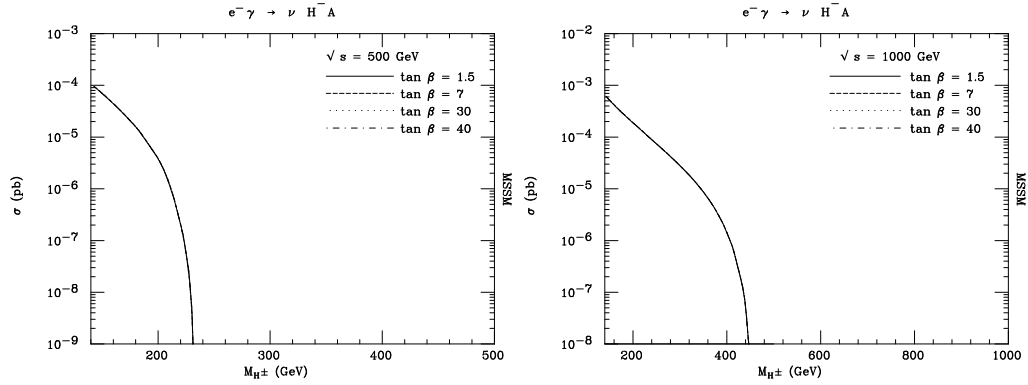
**Figure 5:** Total cross sections for process (1.1).



(a) Process  $e^- \gamma \rightarrow \nu_e \Phi^0 H^-$  with  $\Phi^0 = h^0$ .



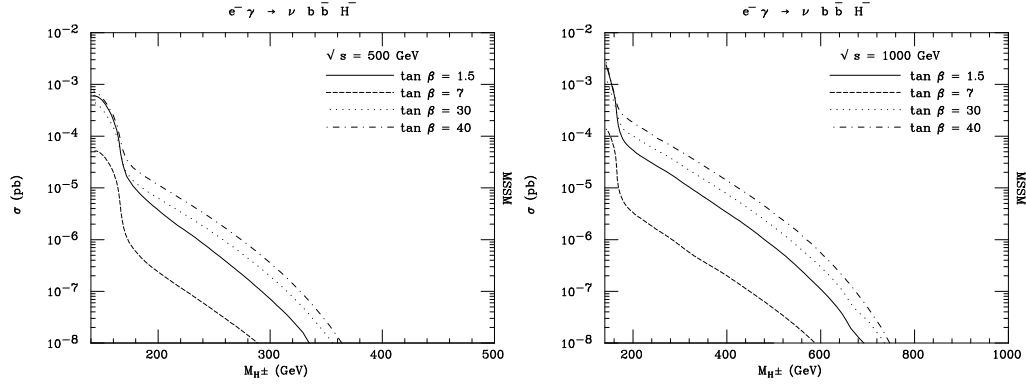
(b) Process  $e^- \gamma \rightarrow \nu_e \Phi^0 H^-$  with  $\Phi^0 = H^0$ .



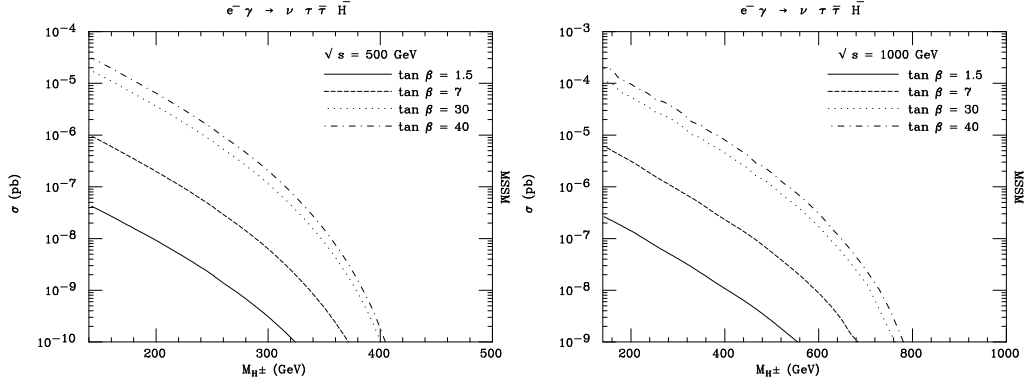
(c) Process  $e^- \gamma \rightarrow \nu_e \Phi^0 H^-$  with  $\Phi^0 = A^0$ .

**Figure 6:** Total cross sections for processes of the type (1.2). In (c), the four curves in each plot coincide within graphical resolution.

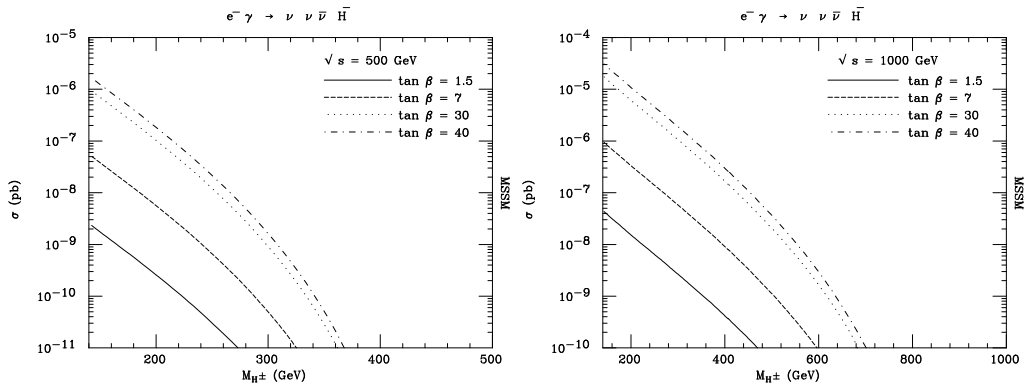




(a) Process  $e^- \gamma \rightarrow \nu_e f \bar{f} H^-$  with  $f = b$ .



(b) Process  $e^- \gamma \rightarrow \nu_e f \bar{f} H^-$  with  $f = \tau$ .



(c) Process  $e^- \gamma \rightarrow \nu_e f \bar{f} H^-$  with  $f = \nu_\tau$ .

**Figure 7:** Total cross sections for processes of the type (1.3).

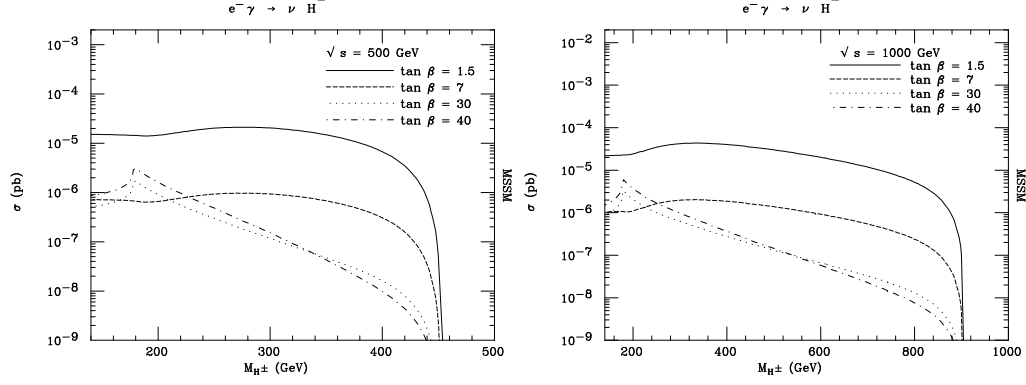


**Figure 8:** Total cross sections for process (1.4).

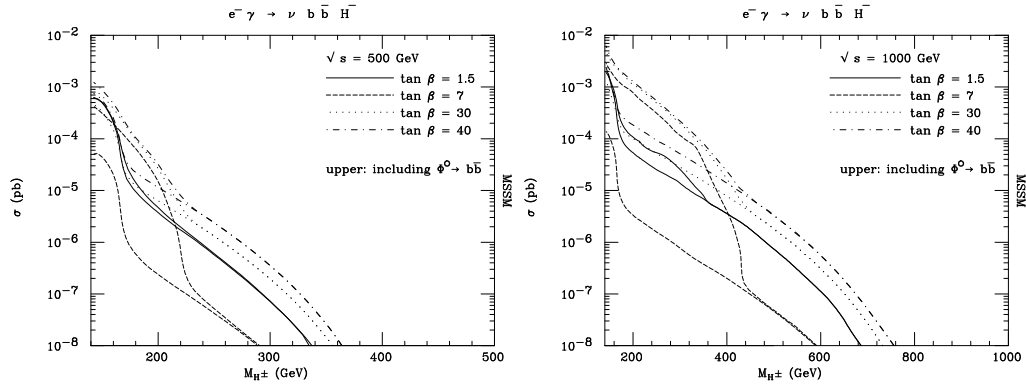


**Figure 9:** Total cross sections for processes of the type (1.2), with  $\Phi^0 \rightarrow b\bar{b}$ , plus those of the type (1.3), with  $f, f' = b, t$ , including the interference (upper curves), compared to the latter only (lower curves).